Article

Effect of Pd-Sensitization on Poisonous Chlorine Gas Detection Ability of TiO₂: Green Synthesis and Low-Temperature Operation

Satish Ekar [1,*], Umesh T. Nakate [2], Yogesh B. Khollam [1], Shoyebmohamad F. Shaikh [3], Rajaram S. Mane [4], Abu ul Hassan S. Rana [5,6,*] and Marimuthu Palaniswami [5]

1 Department of Physics, Baboraoji Gholap College, Pune 411027, Maharashtra, India; ybkhollam@gmail.com
2 Department of Polymer-Nano Science and Technology, Jeonbuk National University, 567 Baekje-daero, Deokjin-gu, Jeonju-si 54896, Jeollabuk-do, Korea; umesh.nakate@gmail.com
3 Department of Chemistry, College of Science, King Saud University, Bld-5, Riyadh 11451, Saudi Arabia; sshaikh1@ksu.edu.sa
4 Centre for Nano-Materials and Energy Devices, School of Physical Sciences, Swami Ramanand Teerth Marathwada University, Nanded 431606, Maharashtra, India; rajarammane70@srtmun.ac.in
5 Department of Electrical and Electronic Engineering, The University of Melbourne, Parkville, VIC 3010, Australia; palani@unimelb.edu.au
6 Department of Obstetrics and Gynaecology, The University of Melbourne, Parkville, VIC 3010, Australia
* Correspondence: satishuekar@gmail.com (S.E.); a.rana@unimelb.edu.au (A.u.H.S.R.)

Abstract: Ganoderma lucidum mushroom-mediated green synthesis of nanocrystalline titanium dioxide (TiO₂) is explored via a low-temperature ($\leq$70 °C) wet chemical method. The role of Ganoderma lucidum mushroom extract in the reaction is to release the ganoderic acid molecules that tend to bind to the Ti^{4+} metal ions to form a titanium-ganoderic acid intermediate complex for obtaining TiO₂ nanocrystallites (NCs), which is quite novel, considering the recent advances in fabricated gas sensing materials. The X-ray powder diffraction, field emission scanning electron microscopy, Raman spectroscopy, and Brunauer–Emmett–Teller measurements etc., are used to characterize the crystal structure, surface morphology, and surface area of as-synthesized TiO₂ and Pd-TiO₂ sensors, respectively. The chlorine (Cl_2) gas sensing properties are investigated from a lower range of 5 ppm to a higher range of 400 ppm. In addition to excellent response–recovery time, good selectivity, constant repeatability, as well as chemical stability, the gas sensor efficiency of the as-synthesized Pd-TiO₂ NC sensor is better (136% response at 150 °C operating temperature) than the TiO₂ NC sensor (57% at 250 °C operating temperature) measured at 100 ppm (Cl_2) gas concentration, suggesting that the green synthesized Pd-TiO₂ sensor demonstrates efficient Cl_2 gas sensing properties at low operating temperatures over pristine ones.

Keywords: bio-synthesis of TiO₂; Cl_2 sensor; Pd-sensitization; low-temperature; selectivity; gas sensor

1. Introduction

Recently, controlling air pollutants and monitoring toxic gases have become increasingly important [1]. Concerns about the environment's health need stringent regulations on the harmful gas emissions from industrial and social sectors. Chlorine (Cl_2), one such toxic gas with a pungent odor, has been a great concern in the past few decades because it is extremely harmful to humans and the environment [2]. Cl_2 molecules can combine with water in the lung mucosa to form hydrofluoric acid when contacted with Cl_2 gas by breathing, causing serious respiratory difficulties. Exposure to high concentrations of Cl_2 is fatal to the human body, irritates the eyes, causes skin infection, psychological disorders, and so on [3]. Cl_2 is widely used in disinfectants, bleach, and raw materials to produce hydrochloric acid, and as part of various industrial processes, including tap water treatment,

paper manufacturing, printing, and dyeing. When Cl_2 is released into the environment without proper treatment, it can be negatively impacted [4]. Considering the growing concern about the hazardous effects of air pollutants, the fabrication and commercialization of low-cost toxic gas sensors is a prime mandate for environmental protection [5].

Over the decades, semiconducting wide band-gap metal oxides have been envisaged in biomedical, water purification, solar cell, chemical and biological sensor applications, and so on [6]. Semiconducting metal oxides such as ZnO [7], SnO_2 [8], WO_3 [9], Fe_2O_3 [10], Bi_2O_3 [11], and so on, have widely been employed in different gas sensor studies. Among them, TiO_2 has gained attention among solid-state sensors due to its low-cost, eco-friendly nature, non-toxic nature, different crystal structures, such as rutile, anatase, and brookite with different chemical, electrical, structural, and optical properties, availability in different dimensions, compatibility, and simplicity of fabrication technology [12,13]. It is an *n*-type semiconducting wide-band gap material with promising applications in gas detection, solar cells, self-cleaning glasses, water purification, and food product industries. It adduces potential biological activities such as anti-fungal, anti-cancer, and anti-microbial. Furthermore, the gas sensing properties of these metal oxide sensors in terms of fast response, low-operating temperature, and good selectivity can be improved by decorating them with nanoparticles of noble metals such as gold (Au), platinum (Pt), and palladium (Pd) [14–16]. Several methods are being established for obtaining TiO_2 nanostructures, such as chemical bath deposition, spray pyrolysis, anodization, sol-gel, hydrothermal, and so on. The bio-inspired metal oxide nanoparticles synthesized using green chemistry demonstrates several advantages over the chemical and physical approaches as this process is; simple (one-pot), low-temperature (70 °C) operating, cost-effective, and environmentally friendly. Furthermore, the abundance and accessibility of biological precursors facilitate large-scale technology development. Green synthesis eliminates the need for additional capping or stabilizing agents, lowering fabrication cost and simplifying the synthetic process. Although green chemistry has several advantages over synthetic chemical approaches, some major concerns must be addressed before these methodologies can be commercialized on a large scale. The main concerns are the possibility of ecological imbalance in natural bioresources due to overuse; differences in active biomolecule/phytochemical concentrations due to seasonal or climate changes, which affect bioactivity or synthesis procedures; and the fact that several nanoparticles (NPs) cannot be prepared using the biosynthesis method due to the requirement of strong reducing agents [17]. Present work is novel in terms of both the green synthesis of TiO_2 nanocrystallites (NCs) and their low-temperature Cl_2 gas sensor application. Efforts have also been taken to enhance the selectivity and gas sensing properties of TiO_2 NCs through Pd-sensitization. Wu et al., prepared Pd-doped mesoporous WO_3 through a hard-templating process with potential hydrogen gas sensing capabilities, such as fast response time, excellent reproducibility, and quick recovery time [18]. The Pd-modified SnO_2 NCs sensor showed improved gas-sensing characteristics, allowing carbon monoxide detection and other extremely low concentration reducing gases such as ethanol and acetone [19]. Suhail et al., obtained a Pd-doped ZnO hydrogen gas sensor; wherein, the doped ZnO film response time of 2–3 s was significantly faster than the traditional ZnO sensor [20]. Pandey et al., investigated the significance of Pd and reduced graphene oxide layers on the gas sensor response of toluene, CO, and ethanol for hydrogen selectivity [21]. At room-temperature, Zhao et al. produced the $CdSnO_3$ gas sensor with improved sensing properties to 1–10 ppm of chlorine gas; the value of gas response was 1338.9 to 5 ppm [22]. Hieu et al., discovered that SnO_2 nanowires are more sensitive to Cl_2 gas than ZnO and WO_3 nanowires. The SnO_2 nanowire sensor that responded to 50 ppb Cl_2 at 50 °C was about 57 [23]. According to Stadler et al., ZnO nanoparticles exhibited a reasonable response of 1278 percent to 200 ppm Cl_2 at 200 °C, with fast response and recovery time periods [24].

In the present work, the TiO_2 sensor is successfully synthesized via a low-temperature (≤70 °C) bio-inspired wet chemical synthesis method in the presence of Ganoderma lucidum mushroom for Cl_2 gas sensing application. The role of Ganoderma lucidum mush-

room extract in the reaction is to release the ganoderic acid molecules, which tend to bind the Ti^{4+} metal ions to form a titanium–ganoderic acid intermediate complex for obtaining TiO_2 NCs. The Pd-sensitization is carried out on the TiO_2 sensor surface by impregnating the Pd-TiO_2 NC sensor. Both TiO_2 and Pd-TiO_2 NC sensors are characterized for their structure and morphology using standard material characterization tools. The gas sensing behaviors of TiO_2 and Pd-TiO_2 NC sensors are investigated for various gases such as ammonia (NH_3), hydrogen sulfide (H_2S), carbon dioxide (CO_2), nitrogen dioxide (NO_2), and chlorine (Cl_2), out of which, Cl_2 has revealed an optimum performance, and therefore, the Cl_2 sensing properties are performed as a function of operating temperature and concentration with error limit. The transient responses for both sensors are also studied to find the respective response and recovery periods. The repeatability and stability tests of both sensor materials are recorded and reported.

2. Materials and Methods

2.1. Materials

The analytical grade titanium (IV) isopropoxide (97%, TTIP), palladium (II) chloride (99%, $PdCl_2$), polyvinyl alcohol (PVA, [-CH_2CHOH-]n), ethyl alcohol(96%, CH_3CH_2OH) are obtained from Sigma Aldrich and utilized as received, without further purification.

2.2. An Extract Preparation

The medicinal Ganoderma lucidum mushroom collected from the forest of Tamhini of Pune District, Maharashtra, India, was washed with distilled water (Milli-Q water; 18.2 MΩ cm) a few times to remove dust and any other parasites that could be present. It was then dried under shade at room-temperature (27 °C) for about fifteen days under dust-free conditions. The mushroom was then divided into fine pieces, grounded, and sieved to get a fine powder. For 15 min, 1.0 gm of fine mushroom powder was boiled in 100 mL of distilled water at 85 °C. The resulting solution was filtered through Whatman paper no. 1 of 42 pore size and stored as a stock solution at 4 °C before use.

2.3. Synthesis of TiO_2 NC Powder

To prepare Ti- precursor, the 0.5 M titanium (IV) isopropoxide was added into 50 mL of ethyl alcohol and distilled water (1:1 proportion). The mushroom extract solution (5 mL) was added into the Ti-precursor solution, and the resulting mixture was stirred for 5 h and maintained at 70 °C by using a hot plate magnetic stirrer. The solution was allowed to cool down to room temperature (27 °C) after vigorous stirring, and the supernatants were removed, leaving a brown-yellow precipitate as a residue. The precipitate was washed several times with ethyl alcohol and distilled water. The color of the precipitate was brown-yellow due to the formation of the titanium-ganoderic acid intermediate compound. The synthesized precipitate was dried at 50 °C overnight. Finally, this fried precipitate was air-annealed at 450 °C for 2 h to improve the crystallinity of white TiO_2 powder before being kept in an airtight container for later usage (Scheme 1). The solid-state sensor film was prepared by dissolving 1.0 g of polyvinyl alcohol (PVA) as a binder in 10 mL of distilled water followed heating the solution to 90 °C while constantly stirring until a transparent viscous gel. The TiO_2 NCs powder was mixed with a few drops of viscous PVA solution in a pestle and mortar. The excess water and binder were vaporized by coating the mixture on the conventional soda-lime glass as a substrate and drying it at 200 °C for 1h. Half of the obtained TiO_2 film sample was considered pristine TiO_2, whereas the remaining half was used for Pd-sensitization as Pd-sensitized TiO_2.

2.4. Growth Mechanism

TiO_2 NCs were synthesized through the hydrolysis of titanium (IV) isopropoxide in the presence of ganoderic acid at 70 °C as follows. The $Ti(OC_3H_7)_4$ reacts with water. The amount of water determines the degree of hydrolysis (i.e., solubility and ionic products), which is high at the degree of saturation where both are nearly the same, and the type

of initial species formed, such as ganoderic acid molecules for binding metal ions, thus influencing the condensation reaction that involves the polymerization of hydrolyzed titanium alkoxides in alcoholic solution to form Ti^{+4} ions in the solution. Thus, the Ti^{+4} ions bound to ganoderic acid legends to form the titanium–ganoderic acid intermediate complex. The titanium–ganoderic acid complex molecules most likely produce a steric hindrance at specific places via hydrogen bonding, helping to control both the particle size and the porous nature of the aggregates. Subsequently, the as-developed titanium-ganoderic acid complex powder was annealed at 450 °C to obtain a very fine-sized TiO_2 NCs powder.
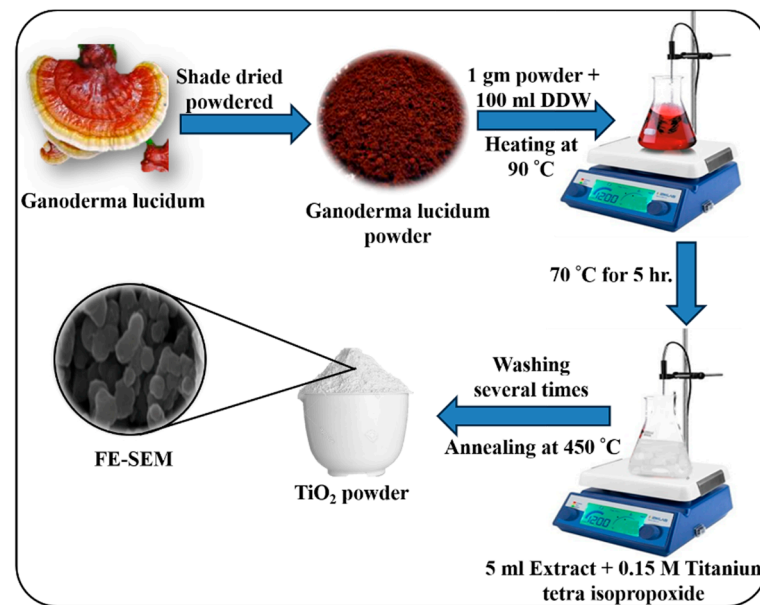
Scheme 1. Schematic presenting a process for obtaining bio-inspired TiO_2 NCs.

2.5. Pd-Sensitized TiO$_2$ NCs

In the present work, Pd-sensitized TiO_2 film was fabricated as follows. The 0.01M $PdCl_2$ in an aqueous solution was used as metal salts for the sensitization of TiO_2 film. The TiO_2 film prepared using the doctor blade method was dipped into a 0.01M aqueous solution of the respective salt for 5 s, and then dried under an IR lamp. Ten such cycles of dipping were carried out for each film. The sensitized TiO_2 film was then heated at 200 °C for 1 h to remove the chloride from the deposited sensor film.

2.6. Characterization Techniques

The field emission scanning electron microscope (FE-SEM, Nova-SEM 200-FEI) was used to confirm the surface morphology of TiO_2, and Pd-TiO_2 sensor film surfaces A FEI TECNAI G2 20 STWIN equipment was used to capture the High-Resolution Transmission Electron Microscopy (HR-TEM) image and electron mapping configuration. The crystal structure was elucidated using an X-ray diffraction (XRD) spectrum (XRD-6000, Shimadzu X-ray diffractometer) and a Cu-K radiation tube. The elemental contents were identified by using an X-ray photoelectron spectroscopy profile obtained on a PHI 5000 Versa Probe (XPS, Ulvac-PHI). Additionally, the Belsorp II, BET, and Japan Inc. equipment measured the surface area and pore-size distribution.

2.7. Gas Sensor Setup

The gas sensing operation was performed in a stainless-steel chamber with 250 mL volume capacity. To adjust the constant temperature, a PID-controlled heater was installed at the base of the cylindrical chamber. To mitigate against changes in operating temperature, a dimmer stat was employed as a stable voltage supply. After adding the target gases to the stainless-steel chamber, a Keithley 6514 programmable computer-connected electrometer

was utilized to identify the sensor film resistance. Thin films with an area of 1.5×1.5 cm^2 were made using a doctor-blade technique on a non-conducting glass substrate in presence of PVA as the binder material which was air-annealed for sensor activity measurement (200 °C, 1 h). The commercial silver paste was used to draw the electrical contacts. The following equation was used to calculate the gas sensor response:

$$S(\%) = \frac{|R_a - R_g|}{R_a} \times 100 \qquad (1)$$

where R_a represents the stabilized resistance of ambient air, R_g represents the stabilized resistance of the target gas.

3. Results and Discussion

3.1. Surface Morphology Appearance

The FE-SEM micrographs of the as-obtained TiO$_2$ and Pd-TiO$_2$ NC film sensors at two different magnifications are shown in Figure 1a,d. The FE-SEM image of the TiO$_2$ film sensor demonstrates the formation of small-sized spherical nanocrystallites with an agglomerated-type architecture. The Pd nanoparticles are uniformly dispersed over the TiO$_2$ film sensor surface in the form of soft agglomerations. Pd nanoparticles show a spillover effect on the surface of the TiO$_2$ film, which is discussed in the below section. The crystal structure and phase analysis of TiO$_2$ and Pd-TiO$_2$ NC sensors characterized by using HR-TEM and HR-TEM techniques are shown in Figure 1b,e. Figure 1b presents the HR-TEM image of TiO$_2$, where the particle size is about 8.0 nm, which was an exact estimation of the XRD (101) peak (i.e., 7.2 nm) using Scherrer relation. Figure 1e provides the HR-TEM image of the Pd-TiO$_2$ sensor where the presence of Pd NCs in the TiO$_2$ matrix is evident. Pd in the form of the cluster along with TiO$_2$ NCs is noticed. The average particle size of the Pd nanocluster (~2 nm) is estimated from the HR-TEM images of Pd-TiO$_2$ NCs (Figure 1e). The surface elemental stoichiometry measured from EDX profile reveals 20.69 and 79.31 percent for the atomic proportions of Ti and O present in the TiO$_2$ film sensor, whereas the mapping proportions for Ti, O, and Pd in Pd-TiO$_2$ are respectively 26.14, 73.15, and 0.71 (Figure 1c,f).
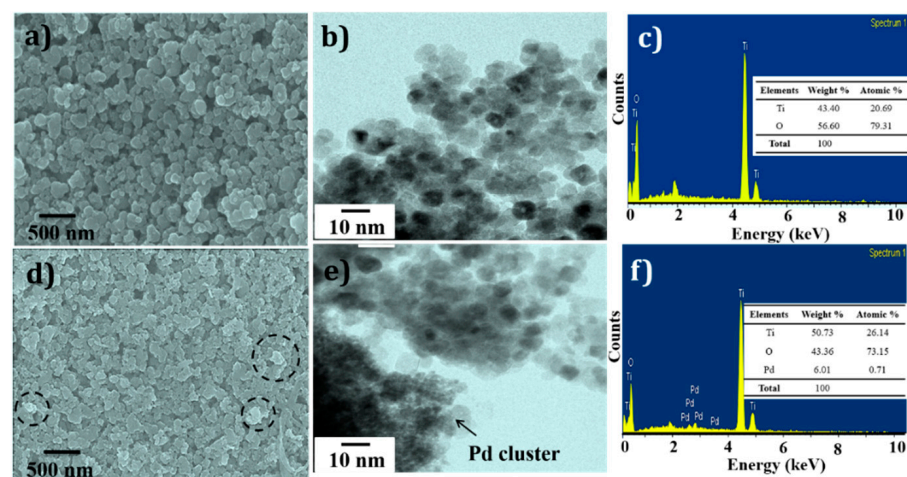

Figure 1. FE-SEM, HR-TEM; elemental analysis of (**a**–**c**), TiO$_2$, and (**d**–**f**); Pd-TiO$_2$ sensor surfaces.

3.2. Structural Elucidation

The XRD patterns of TiO$_2$ and Pd-TiO$_2$ film sensors are shown in Figure 2a. The appearance of the diffraction peaks in the XRD patterns confirms the formation of pyramidal crystal structure with anatase TiO$_2$ phase (JCPDS card No. 21-1272) [25]; however, due to the infinitesimal amount, there is no evolution of diffraction peaks in the XRD pattern for Pd. The sharp diffraction peaks indicate good crystallinity and involvement of no

impurity peaks [26]. The metal oxide gas sensor properties can be influenced by structural parameters such as crystallite size, texture coefficient (TC), and dislocation densities; hence, there is a need to study these parameters of given sensor materials [27–29]. The estimated structural parameters of the as-obtained TiO$_2$ film sensor are tabulated in Table 1. The dislocation densities calculated for each diffraction peak are also given in Table 1. The TC values corresponding to every diffraction peak were estimated. If the TC value is greater than one, sugegsting the preferred orientation. From Table 1, the maximum TC value of 1.22 is associated with the (101) plane, which is the preferred growth direction of the present TiO$_2$ film sensor. The negative value of micro-strain observed in Table 1 infers the existence of compressive type strain. The dislocation densities corresponding to each diffraction peak are mentioned in Table 1.
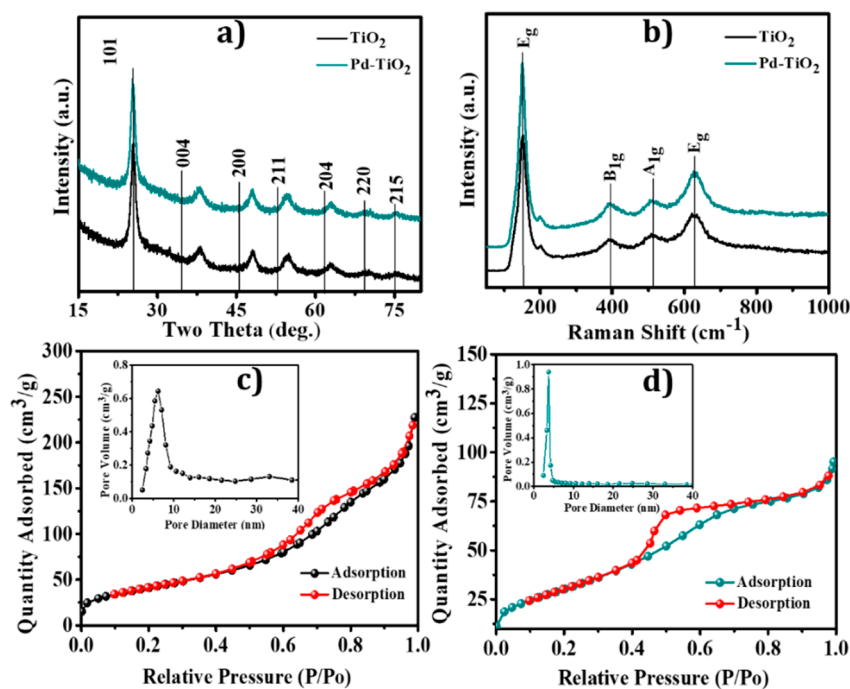

Figure 2. (**a**) XRD patterns, (**b**) Raman spectrums of TiO$_2$ and Pd-TiO$_2$ sensors, and (**c**,**d**) respective BET adsorption–desorption isotherms with pore-size distribution measurements (inset).

Table 1. Structural parameters of TiO$_2$ NCs.

Plane (hkl)	I(hkl)/I0(hkl)	Texture Coefficient	Average Crystal Size D (nm) $D = \frac{K.\lambda}{\beta.cos\theta}$	Micro-Strain $\varepsilon \times 10^{-3}$	Dislocation Density Lines/m^2 $\delta \times 10^{15}$ $\delta = 1/D_2$
(101)	11.61	1.12	8.9	−7.19	12.60
(004)	8.9	0.84	6.8	−6.69	21.60
(105)	10.2	0.99	7.6	−7.35	17.31
(204)	10.0	0.97	5.4	−11.93	34.29

Raman spectroscopy is a powerful technique to detect molecules in TiO$_2$ film sensor obtained from the Ganoderma lucidum mushroom. The significant Raman shift peaks at E$_g$ (144), E$_g$ (205), B$_{1g}$ (400), B$_{1g}$/A$_{1g}$ (519), and E$_g$ (635) cm^{-1}, as shown in Figure 2b, are attributed to the anatase crystal phase of TiO$_2$ [30]. In the Raman spectrum, no additional peaks, except distinctive vibrations, are found, thus confirming the formation of the pure phase of Pd-TiO$_2$. The nitrogen adsorption and desorption isotherms obtained during the BET surface area measurement for pristine TiO$_2$ and Pd-TiO$_2$ films are shown in Figure 2c,d. The specific surface areas for TiO$_2$ and Pd-TiO$_2$ NC film sensors are respectively 161.5 m^2/g

and 170.9 m^2/g. It seems that Pd incorporation decreases the particle size of TiO$_2$, which, in turn, enhances the specific surface area [31]. The insets of Figure 2c,d present the pore-size distribution curves for the pristine TiO$_2$ and Pd-TiO$_2$ NCs sensors. The pore-size distribution is narrow, nearly nano-sized pores, resulting in an average pore volume of 0.15 cm^3/g for pristine TiO$_2$ and 0.17 cm^3/g for Pd-TiO$_2$ NCs. The average pore diameter of the pristine TiO$_2$ and Pd-TiO$_2$ NCs are found to be 7.13 and 4.25 nm, respectively. The higher surface area of pristine TiO$_2$ and Pd-TiO$_2$ NCs and their porous nature may provide access to active sites and a surface for adsorption of target gas molecules to enhance the gas sensing activity.

3.3. Elemental Analysis

The surface states of Pd-TiO$_2$ NCs were investigated by using X-ray photoelectron spectroscopy analysis. The survey XPS spectrum of the Pd-TiO$_2$ film sensor is shown in Figure 3a, confirming the presence of Pd, Ti, and O elements. The high-resolution XPS spectra for Ti2p, O1s, and Pd 3d are shown in Figure 3b–d.
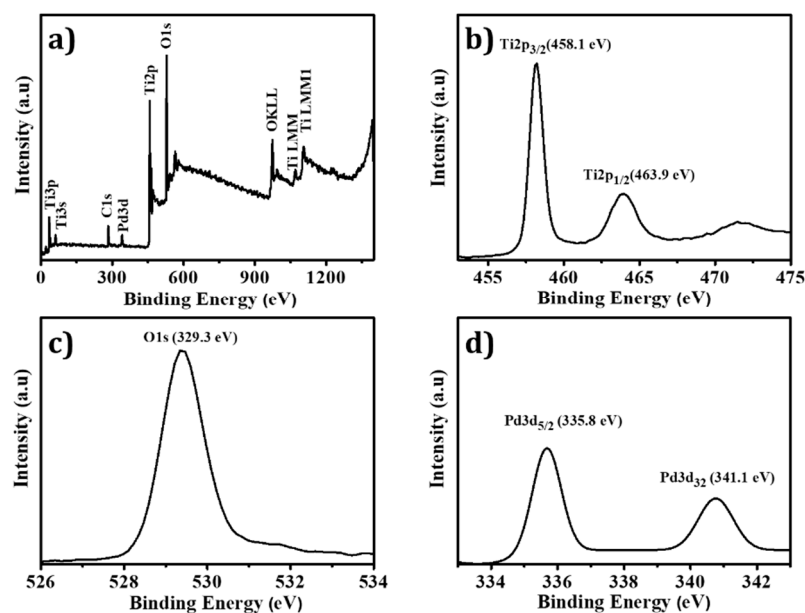

Figure 3. XPS analysis of Pd-TiO$_2$ film sensor; (**a**) survey spectrum, and (**b–d**) high-resolution Ti2p, O1s, and Pd 3d spectrums.

The Ti2p$_{3/2}$ peak has a binding energy of 463.9 eV, whereas the low-intensity Ti2p$_{1/2}$ peak has a binding energy of 458.1 eV, thus indicating the presence of a Ti^{4+} oxidation state [32]. The O1s spectrum of the pristine TiO$_2$ film sensor noted, as seen in Figure 3c at 529.3 eV, is of TiO$_2$ which is ascribed to the surface oxygen atoms [33]. The Pd3d spectrum, as shown in Figure 3d, adduces two peaks: one at 341.1 eV corresponding to Pd3d$_{3/2}$, and the other at 335.8 eV for Pd3d$_{5/2}$. The appearance of Pd^{2+} peak may be due to the partial oxidation of the Pd surface since the Pd particles are very minute in the Pd-TiO$_2$ film sensor [34].

3.4. Gas Sensing Properties

The gas sensing properties of the TiO$_2$ and Pd-TiO$_2$ film sensors were investigated. Metal oxide-based gas sensors usually work at higher operating temperatures (i.e., $\geq$150 °C). The adsorption/desorption of target gas molecules varies with the operating temperature. As a result, optimizing the current sensor's operating temperature is critical. These TiO$_2$ and Pd-TiO$_2$ sensors were studied for Cl$_2$ (100 ppm) at various operating temperatures (Figure 4a). It was observed that the TiO$_2$ film sensor reveals the highest Cl$_2$ response of 57%, at a 250 °C operating temperature. In contrast, the Pd-TiO$_2$ film sensor demonstrates

the highest Cl_2 response at 136%, at a relatively low operating temperature (i.e., 150 °C). The involvement of oxygen vacancies, which act as defects, is responsible for an *n*-type semiconducting behavior of TiO_2; hence, electrons are the majority charge carriers in the conduction band. The basis for sensor working is the change of its resistance on the exposure of the target gas. The resistance of the TiO_2 NCs film sensor is increased after Cl_2 gas exposure. A typical Cl_2 gas sensing mechanism has been explained for *n*-type metal oxide-based gas sensor by Navale et al. [24]. The presence of the Pd catalyst on the TiO_2 surface is responsible for the higher Cl_2 gas response at the relatively low optimal operating temperature [15]. Pd (being noble metal) has better dissociation catalytic ability.
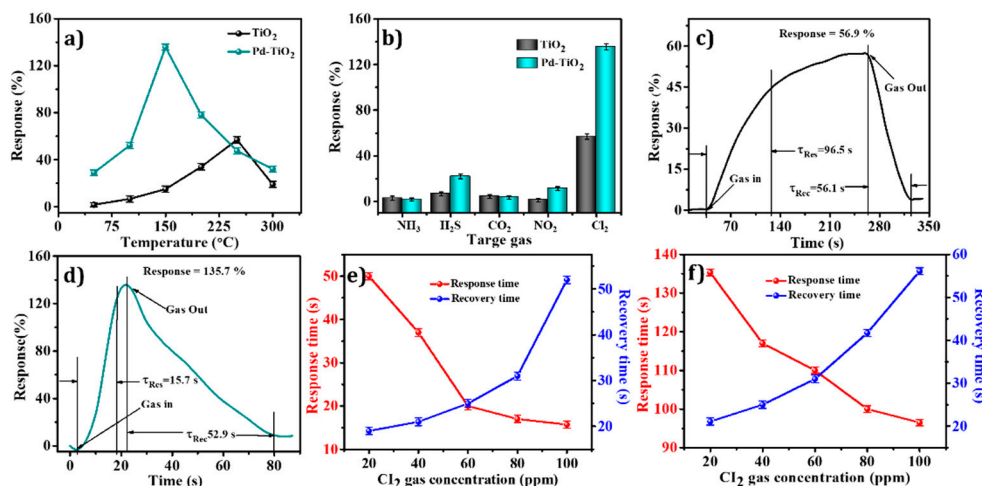

Figure 4. (**a**) Gas response (at different operating temperatures); (**b**) selectivity of sensors for various gases; (**c**,**d**) response and recovery measurements at 100 ppm of Cl_2 gas; and (**e**,**f**) response vs. recovery plots for Cl_2 gas at different concentrations (from 20 to 100 ppm) of TiO_2 and Pd-TiO_2.

The presence of Pd catalyst on the sensor surface provides an active site and surface to enhance the catalytic chemical sensing reaction. The electrical and chemical effects of the Pd catalyst help to improve the gas sensing performance [35]. As well as Cl_2, these sensors are further employed to check their responses to gases such as NH_3, H_2S, CO_2, and NO_2 (Figure 4b). Both sensors feature good selectivity towards Cl_2 gas, whereas the Pd-TiO_2 NCs film sensor reveals higher selectivity over the TiO_2 film sensor. The transient Cl_2 gas responses for TiO_2 and Pd-TiO_2 film sensors are provided in Figure 4c,d. As the Cl_2 gas is injected into the testing system, the target gas molecules diffuse through air and get adsorbed onto the sensor surface for catalytic sensing reaction over time. This sensor shows the response in increasing order as time progresses until saturation or equilibrium level for a given target gas concentration is achieved.

At the saturation level, the sensor shows a constant response. After the gas testing system is opened to an outer atmosphere, the target gas molecules start desorbing, and the corresponding sensor response also decreases. The time taken by the sensor to reach 90% of the change in response or resistance value for a given concentration of target gas is nothing but the response time. Similarly, recovery time can also be recorded. The recorded response time values for TiO_2 and Pd-TiO_2 sensors are respectively 96.5 s and 15.7 s. The recovery time values for TiO_2 and Pd-TiO_2 sensors are 56.1 s and 52.9 s, respectively, which are approximately the same. The fast response of the Pd-TiO_2 NC film sensor is attributed to the fast Cl_2 gas sensing catalytic reaction on the sensor surface in the presence of Pd. The repeatability and transient gas response studies for increasing the target gas concentration of TiO_2 and Pd-TiO_2 sensors are given in Figure 4e,f. In Figure 4f, the response time decreases from 135 to 96.5 s for the Pd-TiO_2 NC film sensor, whereas recovery time increases from 21 to 56 s with an increase of Cl_2 gas concentration from 20 to 100 ppm. The decrease in response time is attributed to the abundance of vacant sites on the film surface for gas adsorption. At the same time, the increase in recovery time is assigned to the heavier nature

of Cl_2 gas. Moreover, this may be due to the reaction products that are not leaving the interface immediately after the reaction, thus resulting in a decrease in desorption rate [36].

3.5. Effect of Cl_2 Gas Concentration on Sensor Response

Figure 5a,b depict the dynamic gas responses of the TiO_2 and $Pd-TiO_2NCs'$ film sensors vs. time towards 5–400 ppm concentrations of Cl_2 gas. The response values of the TiO_2 sensor toward 5, 20, 40, 100, 200, and 400 ppm concentrations of Cl_2 gas at 250 °C are found to be 17.14, 40.8, 49.6, 56.9, 62.7, 68.2, and 70.4%, respectively. It is observed that, as the concentration of Cl_2 increases, the TiO_2 film sensor response also increases; this is because higher Cl_2 gas concentration covers the higher surface of the TiO_2 film sensor, eventually increasing the interaction between Cl_2 gas molecules and sensor surface. On the other hand, lower Cl_2 gas concentration mitigates the interaction between Cl_2 gas molecules and the sensor surface; a lower response is obtained due to the lower surface coverage [37]. Moreover, from Figure 5b, the $Pd-TiO_2$ NC film sensor can detect as low as 5 ppm Cl_2 gas with a phenomenal response of 40.3%. Both the sensors demonstrate a lower gas response for lower Cl_2 gas concentration. With an increase in Cl_2 concentration, corresponding, responses are also increased (168.5% at 400 ppm). The response to maximum Cl_2 gas concentration is restricted by the available area of the sensor surface. As the sensor surface area is limited, the sensor gets saturated, indicating a saturated response for higher gas concentrations [38].
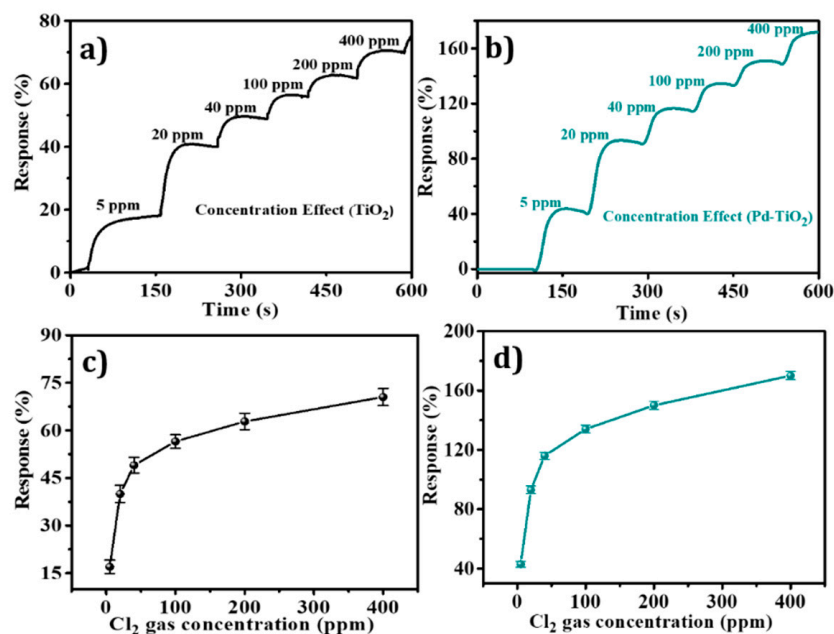

Figure 5. (**a**,**b**) Dynamic response–recovery characteristic curves at different Cl_2 gas concentrations (from 5 to 400 ppm) and (**c**,**d**) exponential relationship (between gas response and gas concentration) of TiO_2 and $Pd-TiO_2$ NC film sensors.

As shown in Figure 5c,d, the exponential relationship between gas response and gas concentration—tested three times—reveals good reproducibility for both sensors. At lower concentrations, the Cl_2 gas molecules cover a smaller portion of the surface of sensitized sensor films, resulting in fewer surface interactions and, as a result, a smaller response value is noted. Furthermore, a higher concentration of Cl_2 gas covers more sensor surface area, resulting in a higher response value due to greater surface contacts [39]. The Cl_2 gas sensing performance of the $Pd-TiO_2$ NCs sensor was compared with previously published data (shown in Table 2).

Table 2. Comparison of responses of different material-based Cl_2 gas sensors found in the literature. (C = Concentration (ppm), S = Response, T = Temperature (°C), RT = Room temperature).

Material	Synthesis Method	Gas	S	C	T (°C)	Ref.
$CdSnO_3$	Hydrothermal	Cl_2	1338.9 *	5 ppm	RT	[22]
SnO_2	Chemical vapor deposition	Cl_2	57 *	50 ppb	50 °C	[23]
ZnO	Rapid solid-state	Cl_2	1278%	200 ppm	200 °C	[24]
Pd-TiO$_2$	**Wet chemical**	**Cl_2**	**136%**	**100 ppm**	**150 °C**	**This Work**

* The Response value calculated using formula $S = R_a/R_g$.

3.6. Reproducibility and Stability Studies

The reliability and quality studies of the film sensors are represented by two important parameters; reproducibility and stability. The capability of sensor material to reproduce the same experimental results measured for another synthesis batch under similar working environmental conditions is reproducibility. To study the reproducibility of the TiO_2 film sensor, three sensor scans were operated to 100 ppm of Cl_2 gas in the same working environment (Figure 6a). The reproducibility of a sensor is one of the measures of its product quality. To investigate the reproducibility of the Pd-TiO$_2$ NCs; film, response experiments were repeated three times towards a 100 ppm of Cl_2. The results in Figure 6b demonstrate that upon repeated exposure to 100 ppm Cl_2 gas, the response of the Pd-TiO$_2$ NCs film sensor is almost constant, which confirms the excellent repeatability of the Pd-sensitized sensor material [40]. Response stability is one of the most important parameters of metal oxide-based gas sensors; therefore, the stability studies of both TiO_2 and Pd-TiO$_2$ NCs film sensors were studied towards the fixed 100 ppm concentration of Cl_2 gas for thirty days at five days (Figure 6c). Both the sensors retain the responses significantly for thirty days; however, the Pd-TiO$_2$ film sensor has confirmed the highest stability response (92.0%) to 100 ppm Cl_2 gas concentration at 150 °C, thus signifying its excellent chemical and environmental stability.
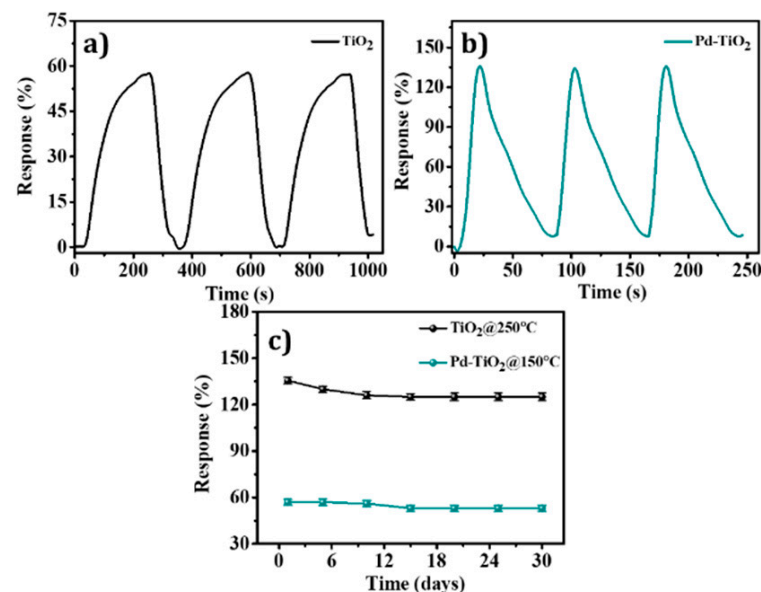

Figure 6. (**a**,**b**) Three response curves, and (**c**) long-term stability curve at 100 ppm Cl_2 gas concentration of TiO_2 and Pd-TiO$_2$ film sensors.

3.7. Gas Sensor Working Mechanism

The most widely prevalent gas sensor working mechanism for *n*-type metal oxide films is the sensor materials' noteworthy resistance change, which is caused by the adsorption/desorption process of the gas molecules on the sensing materials' surface during

exposure to various gas environments [41]. Based on the energy band diagram, as given in Scheme 2, a gas sensing mechanism of the Pd-TiO$_2$ film sensor in the presence of air atmosphere and Cl$_2$ gas has been proposed. The majority charge carrier in the *n*-type Pd-TiO$_2$ semiconductor is electrons. Under ambient air conditions, oxygen molecules are adsorbed on the Pd-TiO$_2$ film's exposed surface by capturing electrons from the TiO$_2$ valance band. The process creates a surface depletion layer via adsorbed oxygen species (O$^-$).
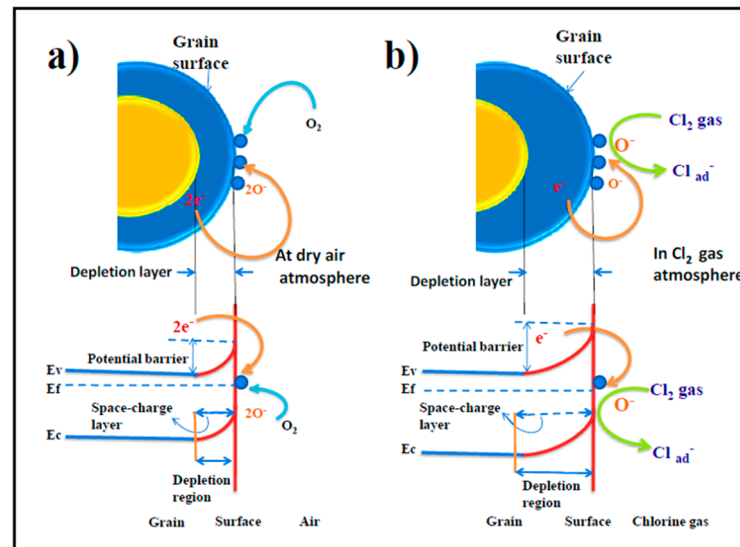
Scheme 2. (**a,b**) Proposed sensing-based reaction mechanism for the Pd-TiO$_2$ NC film sensor in air and Cl$_2$ gas atmospheres.

The resistance of the sensor films changes when oxygen is absorbed on the sensor surface. Generally, the adsorbed oxygen ion species depend on the sensor film temperature, with O^{2-} below 100 °C, O$^-$ in between 100–300 °C, and O^{2-} above 300 °C [42]. O$^-$ is dominant in the present study because of the approximate Pd-TiO$_2$ film's working temperature of 150 °C. From Scheme 2, it is seen that the potential barrier has a direct relationship with the oxygen ions on the film surface. The increase in potential barrier height eventually increases the film resistance. When the sensors are exposed to oxidizing gas, such as Cl$_2$, Cl$_2$ gas molecules react with oxygen ions to form ClO$^-$ species, and conduction electrons (drawn from Pd-TiO$_2$ film) confirm Cl$_{ad}{}^-$. This decreases the film's carrier concentration, thus increasing the depletion width and film resistance. The proposed reaction is as follows:

$$\frac{1}{2}Cl_2 + e^- \rightarrow Cl_{ad}{}^- \tag{2}$$

$$\frac{1}{2}Cl_2 + V_O + e^- \rightarrow ClO^- \tag{3}$$

where subscripts ad$^-$ and O$^-$ denotes species adsorbed on the surface of the film sensor and species occupy lattice oxygen sites, respectively, and Vo is oxygen vacancy [27,43]. The proposed gas sensing mechanism of the Pd-TiO$_2$ NCs' film sensor for the Cl$_2$ gas atmosphere is shown in Scheme 2b. Noble metals such as Au, Pt, Ag, and Pd are frequently used as sensitizers in sensing materials to improve their gas sensing properties [44]. The enhanced gas sensing properties of nobel metal doped sensing materials are due to two effects; electronic sensitization and chemical sensitization [45]. To begin, in the case of the electron sensitization effect, free electron transfer between Pd and TiO$_2$ occurs due to their different work functions, resulting in the formation of a Schottky barrier and extra electron depleted layers near the contact interfaces. When the Cl$_2$ gas molecules come into contact with the sensing material, the extra electron depleted layer causes an increasing number of Cl$_2$ molecules to be adsorbed on the sensor surface, thus increasing the gas sensor response. Second, the active Pd nanoparticles accelerate the reaction by providing more active sites

for Cl_2 gas molecules to interact with, which may be one of the factors responsible for improved sensor performance.

4. Conclusions

In summary, the nanocrystalline TiO_2 film sensor has been synthesized by a low-temperature ($\leq 70\,^\circ$C) bio-inspired wet chemical method in Ganoderma lucidum mushroom sensitized with Pd as Pd-TiO_2 sensor by a simple dip-coating method. Both the sensors endow a good selectivity for Cl_2 gas. The slow response/recovery time and high operating temperature are also major drawbacks of Cl_2-based gas sensors. To overcome this disadvantage, Pd doping in TiO_2 produces a synergetic effect that improves response/recovery time and lowers operating temperature. The TiO_2 sensor shows the highest Cl_2 gas response of 57% for 100 ppm at 250 °C operating temperature. The Pd-TiO_2 film sensor exhibits the highest Cl_2 gas response of 136% at the relatively lower operating temperature of 150 °C. The response/recovery time for the TiO_2 sensor is 97 s/56 s, whereas it is just 16 s/52 s for the Pd-TiO_2 film sensor. At a concentration of 5 ppm, Cl_2 detection is smaller, whereas, at a concentration of 400 ppm, Cl_2 detection is higher. The present sensors reveal a good response–recovery properties, selectivity, remarkable repeatability, and stability for Cl_2 sensing; therefore, bio-inspired wet chemical synthesis of TiO_2 in the presence of Ganoderma lucidum mushroom can be a potential candidate, over other expensive and rare-earth materials, for obtaining TiO_2 and Pd-TiO_2 film sensors which would be an easy way to increase the sensitivity of Cl_2 for producing scalable commercial gas sensors.

Author Contributions: Conceptualization, S.E., S.F.S. and A.u.H.S.R.; data curation, U.T.N.; formal analysis, S.E., U.T.N., Y.B.K., S.F.S., R.S.M., A.u.H.S.R. and M.P.; funding acquisition, S.F.S.; investigation, S.E., U.T.N., R.S.M., A.u.H.S.R. and M.P.; methodology, S.E., and Y.B.K.; Project administration, S.F.S. and R.S.M.; resources, R.S.M. and M.P.; software, U.T.N. and Y.B.K.; supervision, R.S.M., A.u.H.S.R. and M.P.; validation, A.u.H.S.R. and M.P.; writing—original draft, S.E.; writing—review and editing, U.T.N., Y.B.K., S.F.S., R.S.M., A.u.H.S.R. and M.P. All authors have read and agreed to the published version of the manuscript.

Institutional Review Board Statement: Not applicable.

Informed Consent Statement: Not applicable.

Data Availability Statement: Not applicable.

Conflicts of Interest: The authors declare no conflict of interest.

References

1. Cozma, A.; Firculescu, A.-C.; Tudose, D.; Ruse, L. Autonomous Multi-Rotor Aerial Platform for Air Pollution Monitoring. *Sensors* **2022**, *22*, 860. [CrossRef]
2. Ma, J.; Fan, H.; Zhang, W.; Sui, J.; Wang, C.; Zhang, M.; Zhao, N.; Kumar Yadav, A.; Wang, W.; Dong, W.; et al. High Sensitivity and Ultra-Low Detection Limit of Chlorine Gas Sensor Based on In_2O_3 Nanosheets by a Simple Template Method. *Sens. Actuators B Chem.* **2020**, *305*, 127456. [CrossRef]
3. Waghmare, S.D.; Raut, S.D.; Ghule, B.G.; Jadhav, V.V.; Shaikh, S.F.; Al-Enizi, A.M.; Ubaidullah, M.; Nafady, A.; Thamer, B.M.; Mane, R.S. Pristine and palladium-doped perovskite bismuth ferrites and their nitrogen dioxide gas sensor studies. *J. King Saud Univ.-Sci.* **2020**, *32*, 3125–3130. [CrossRef]
4. Li, Q.; Zhang, W.; Wang, C.; Ma, J.; Ning, L.; Fan, H. Ag Modified Bismuth Ferrite Nanospheres as a Chlorine Gas Sensor. *RSC Adv.* **2018**, *8*, 33156–33163. [CrossRef]
5. Cano, M.; Castillero, P.; Roales, J.; Pedrosa, J.M.; Brittle, S.; Richardson, T.; González-Elipe, A.R.; Barranco, A. A transparent TMPyP/TiO_2 composite thin film as an HCl sensitive optochemical gas sensor. *Sens. Actuators B Chem.* **2010**, *150*, 764–769. [CrossRef]
6. Chavali, M.S.; Nikolova, M.P. Metal Oxide Nanoparticles and Their Applications in Nanotechnology. *SN Appl. Sci.* **2019**, *1*, 607. [CrossRef]

7. Zhang, Y.; Liu, C.; Gong, F.; Jiu, B.; Li, F. Large Scale Synthesis of Hexagonal Simonkolleit Nanosheets for ZnO Gas Sensors with Enhanced Performances. *Mater. Lett.* **2017**, *186*, 7–11. [CrossRef]

8. Liu, Y.; Huang, J.; Yang, J.; Wang, S. Pt Nanoparticles Functionalized 3D SnO$_2$ Nanoflowers for Gas Sensor Application. *Solid-State Electron.* **2017**, *130*, 20–27. [CrossRef]

9. Shaikh, S.F.; Ghule, B.G.; Shinde, P.V.; Raut, S.D.; Gore, S.K.; Ubaidullah, M.; Mane, R.S.; Al-Enizi, A.M. Continuous Hydrothermal Flow-Inspired Synthesis and Ultra-Fast Ammonia and Humidity Room-Temperature Sensor Activities of {WO}$_3$ Nanobricks. *Mater. Res. Express* **2020**, *7*, 15076. [CrossRef]

10. Ghule, B.G.; Shinde, N.M.; Raut, S.D.; Gore, S.K.; Shaikh, S.F.; Ekar, S.U.; Ubaidullah, M.; Pak, J.J.; Mane, R.S. Self-Assembled α-Fe$_2$O$_3$-GO Nanocomposites: Studies on Physical, Magnetic and Ammonia Sensing Properties. *Mater. Chem. Phys.* **2022**, *278*, 125617. [CrossRef]

11. Ghule, B.G.; Shinde, N.M.; Raut, S.D.; Shaikh, S.F.; Al-Enizi, A.M.; Kim, K.H.; Mane, R.S. Porous Metal-Graphene Oxide Nanocomposite Sensors with High Ammonia Detectability. *J. Colloid Interface Science* **2021**, *589*, 401–410. [CrossRef] [PubMed]

12. Shaikh, S.F.; Ghule, B.G.; Nakate, U.T.; Shinde, P.V.; Ekar, S.U.; O'Dwyer, C.; Kim, K.H.; Mane, R.S. Author Correction: Low-Temperature Ionic Layer Adsorption and Reaction Grown Anatase TiO$_2$ Nanocrystalline Films for Efficient Perovskite Solar Cell and Gas Sensor Applications. *Sci. Rep.* **2019**, *9*, 8432. [CrossRef] [PubMed]

13. Shaikh, S.F.; Mane, R.S.; Min, B.K.; Hwang, Y.J.; Joo, O. D-Sorbitol-Induced Phase Control of TiO$_2$ Nanoparticles and Its Application for Dye-Sensitized Solar Cells. *Sci. Rep.* **2016**, *6*, 20103. [CrossRef]

14. Zou, A.L.; Qiu, Y.; Yu, J.J.; Yin, B.; Cao, G.Y.; Zhang, H.Q.; Hu, L.Z. Ethanol Sensing with Au-Modified ZnO Microwires. *Sens. Actuators B Chem.* **2016**, *227*, 65–72. [CrossRef]

15. Şennik, E.; Alev, O.; Öztürk, Z.Z. The Effect of Pd on the H2 and VOC Sensing Properties of TiO$_2$ Nanorods. *Sens. Actuators B Chem.* **2016**, *229*, 692–700. [CrossRef]

16. Samerjai, T.; Liewhiran, C.; Wisitsoraat, A.; Tuantranont, A.; Khanta, C.; Phanichphant, S. Highly Selective Hydrogen Sensing of Pt-Loaded WO$_3$ Synthesized by Hydrothermal/Impregnation Methods. *Int. J. Hydrog. Energy* **2014**, *39*, 6120–6128. [CrossRef]

17. Jayaseelan, C.; Rahuman, A.A.; Roopan, S.M.; Kirthi, A.V.; Venkatesan, J.; Kim, S.-K.; Iyappan, M.; Siva, C. Biological Approach to Synthesize TiO$_2$ Nanoparticles Using Aeromonas Hydrophila and Its Antibacterial Activity. *Spectrochim. Acta Part A Mol. Biomol. Spectrosc.* **2013**, *107*, 82–89. [CrossRef]

18. Wu, C.-H.; Zhu, Z.; Huang, S.-Y.; Wu, R.-J. Preparation of Palladium-Doped Mesoporous WO$_3$ for Hydrogen Gas Sensors. *J. Alloy. Compd.* **2018**, *776*, 965–973. [CrossRef]

19. Wang, Q.; Wang, C.; Sun, H.; Sun, P.; Wang, Y.; Lin, J.; Lu, G. Microwave Assisted Synthesis of Hierarchical Pd/SnO$_2$ Nanostructures for CO Gas Sensor. *Sens. Actuators B Chem.* **2016**, *222*, 257–263. [CrossRef]

20. Rashid Saleh, W.; Al-zaidi, Q.; Suhail, A. Palladium—Doped ZnO Thin Film Hydrogen Gas Sensor. *Appl. Phys. Res.* **2011**, *3*, 89. [CrossRef]

21. Pandey, P.; Wilson, N.; Covington, J. Pd-Doped Reduced Graphene Oxide Sensing Films for H$_2$ Detection. *Sens. Actuators B Chem.* **2013**, *183*, 478–487. [CrossRef]

22. Zhao, X.; Li, Z.; Lou, X.; Li, M.; Zhang, N. Room-temperature chlorine gas sensor based on CdSnO$_3$ synthesized by hydrothermal process. *J. Adv. Ceram.* **2013**, *2*, 31–36. [CrossRef]

23. Dang, T.V.; Hoa, N.D.; Duy, N.V.; Hieu, N.V. Chlorine Gas Sensing Performance of On-chip Grown ZnO, WO$_3$, and SnO$_2$ Nanowire Sensors. *ACS Appl. Mater. Interfaces* **2016**, *8*, 4828–4837. [CrossRef] [PubMed]

24. Navale, S.T.; Jadhav, V.V.; Tehare, K.K.; Sagar, R.U.R.; Biswas, C.S.; Galluzzi, M.; Liang, W.; Patil, V.B.; Mane, R.S.; Stadler, F.J. Solid-state synthesis strategy of ZnO nanoparticles for the rapid detection of hazardous Cl$_2$. *Sens. Actuators B Chem.* **2017**, *38*, 1102–1110. [CrossRef]

25. Wang, D.; He, Y.; Zhong, N.; He, Z.; Shen, Y.; Zeng, T.; Lu, X.; Ma, J.; Song, S. In situ chloride-mediated synthesis of TiO$_2$ thin film photoanode with enhanced photoelectrochemical activity for carbamazepine oxidation coupled with simultaneous cathodic H$_2$ production and CO$_2$ conversion to fuels. *J. Hazard. Mater.* **2021**, *410*, 124563. [CrossRef]

26. Noor, S.; Sajjad, S.; Leghari, S.A.K.; Flox, C.; Ahmad, S. Competitive Role of Nitrogen Functionalities of N Doped GO and Sensitizing Effect of Bi$_2$O$_3$ QDs on TiO$_2$ for Water Remediation. *J. Environ. Sci.* **2021**, *108*, 107–119. [CrossRef]

27. Xu, C.; Tamaki, J.; Miura, N.; Yamazoe, N. Grain Size Effects on Gas Sensitivity of Porous SnO$_2$-Based Elements. *Sens. Actuators B Chem.* **1991**, *3*, 147–155. [CrossRef]

28. Kumar, M.; Kumar, A.; Abhyankar, A.C. Influence of Texture Coefficient on Surface Morphology and Sensing Properties of W-Doped Nanocrystalline Tin Oxide Thin Films. *ACS Appl. Mater. Interfaces* **2015**, *7*, 3571–3580. [CrossRef]

29. Jiménez, I.; Arbiol, J.; Dezanneau, G.; Cornet, A.; Morante, J.R. Crystalline Structure, Defects and Gas Sensor Response to NO$_2$ and H$_2$S of Tungsten Trioxide Nanopowders. *Sens. Actuators B Chem.* **2003**, *93*, 475–485. [CrossRef]

30. Challagulla, S.; Tarafder, K.; Ganesan, R.; Roy, S. Structure Sensitive Photocatalytic Reduction of Nitroarenes over TiO$_2$. *Sci. Rep.* **2017**, *7*, 8783. [CrossRef]

31. Seifvand, N.; Kowsari, E. Synthesis of Mesoporous Pd-Doped TiO$_2$ Templated by a Magnetic Recyclable Ionic Liquid for Efficient Photocatalytic Air Treatment. *Ind. Eng. Chem. Res.* **2016**, *55*, 10533–10543. [CrossRef]

32. Nawaz, R.; Kait, C.F.; Chia, H.K.; Isa, M.H.; Lim, W. Glycerol-Mediated Facile Synthesis of Colored Titania Nanoparticles for Visible Light Photodegradation of Phenolic Compounds. *Nanomaterials* **2019**, *9*, 1586. [CrossRef] [PubMed]

33. DeBenedetti, W.J.I.; Hines, M.A. Photochemical Fluorination of TiO$_2$(110) Produces an Atomically Thin Passivating Layer. *J. Phys. Chem. C* **2022**, *126*, 4899–4906. [CrossRef]

34. Liu, S.; Deng, Y.; Fu, L.; Huang, L.; Ouyang, L.; Yuan, S. Understanding the Role of Boron on the Interface Modulation of the Pd/TiO$_2$ Catalyst for Direct Synthesis of H$_2$O$_2$. *ACS Sustain. Chem. Eng.* **2022**, *10*, 3264–3275. [CrossRef]

35. Salunkhe, R.R.; Dhawale, D.S.; Patil, U.M.; Lokhande, C.D. Improved Response of CdO Nanorods towards Liquefied Petroleum Gas (LPG): Effect of Pd Sensitization. *Sens. Actuators B Chem.* **2009**, *136*, 39–44. [CrossRef]

36. Khuspe, G.; Sakhare, R.D.; Navale, S.; Chougule, M.; Kolekar, Y.; Mulik, R.; Pawar, R.; Lee, C.; Patil, D.V. Nanostructured SnO$_2$ Thin Films for NO$_2$ Gas Sensing Applications. *Ceram. Int.* **2013**, *39*, 8673–8679. [CrossRef]

37. Samerjai, T.; Tamaekong, N.; Liewhiran, C.; Wisitsoraat, A.; Phanichphant, S. NO$_2$ Gas Sensing of Flame-Made Pt-Loaded WO$_3$ Thick Films. *J. Solid State Chem.* **2013**, *2014*, 47–52. [CrossRef]

38. Tabassum, R.; Mishra, S.K.; Gupta, B.D. Surface Plasmon Resonance-Based Fiber Optic Hydrogen Sulphide Gas Sensor Utilizing Cu–ZnO Thin Films. *Phys. Chem. Chem. Phys.* **2013**, *15*, 11868–11874. [CrossRef]

39. Huang, X.; Meng, L.; Du, M.; Li, Y. TiO$_2$ Nanorods: Hydrothermal Fabrication and Photocatalytic Activities. *J. Mater. Sci. Mater. Electron.* **2016**, *27*, 7222–7226. [CrossRef]

40. Dey, A. Semiconductor Metal Oxide Gas Sensors: A Review. *Mater. Sci. Eng. B* **2018**, *229*, 206–217. [CrossRef]

41. Skubal, L.R.; Meshkov, N.K.; Vogt, M.C. Detection and identification of gaseous organics using a TiO$_2$ sensor. *J. Photochem. Photobiol. A Chem.* **2002**, *148*, 103–108. [CrossRef]

42. Hong, T.; Culp, J.T.; Kim, K.-J.; Devkota, J.; Sun, C.; Ohodnicki, P.R. State-of-the-Art of Methane Sensing Materials: A Review and Perspectives. *TrAC Trends Anal. Chem.* **2020**, *125*, 115820. [CrossRef]

43. Shinde, V.; Gujar, T.; Lokhande, C. Enhanced Response of Porous ZnO Nanobeads towards LPG: Effect of Pd Sensitization. *Sens. Actuators B Chem.* **2007**, *123*, 701–706. [CrossRef]

44. Hwang, J.; Jung, H.; Shin, H.S.; Kim, D.S.; Kim, D.S.; Ju, B.K.; Chun, M.P. The Effect of Noble Metals on Co Gas Sensing Properties of In$_2$O$_3$ Nanoparticles. *Appl. Sci.* **2021**, *11*, 4903. [CrossRef]

45. Yin, Y.; Shen, Y.; Zhao, S.; Bai, J.; Qi, Y.; Han, C.; Wei, D. Effect of noble metal elements on ethanol sensing properties of ZnSnO$_3$ nanocubes. *J. Alloy. Compd.* **2021**, *887*, 161409. [CrossRef]